Science Translational Medicine
AAAS

Supplementary Materials for

Reactive oxygen species–degradable polythioketal urethane foam dressings to promote porcine skin wound repair

Prarthana Patil *et al.*

Corresponding author: Craig L. Duvall, craig.duvall@vanderbilt.edu

Sci. Transl. Med. **14**, eabm6586 (2022)
DOI: 10.1126/scitranslmed.abm6586

The PDF file includes:

Other Supplementary Material for this manuscript includes the following:

Supplementary Materials

Synthesis of EG0 (BDT), EG1 (MEE), and EG2 (EDDT) PTK diols

All chemical reagents were purchased form Sigma Aldrich. EG0, EG1 and EG2 PTK diols were synthesized as previously published by Martin et al. (*34*, *36*). 1,4 butanedithiol (BDT, EG0), mercaptoethyl ether (MEE, EG1), and 2,2'-(ethylenedioxy) diethanethiol (EDDT, EG2) were polymerized with dimethoxy propane (DMP) through a condensation reaction using *p*-toluene sulphonic acid (pTSA) as a catalyst (fig. S1). First, pTSA was dissolved in concentrated hydrochloric acid (HCl) and heated to 50°C. The acid was allowed to cool, and pTSA crystals were collected, rinsed with cold HCl, and vacuum dried for 2 hours. A tri-neck flask attached with an addition funnel was charged with anhydrous acetonitrile (ACN) and dithiol monomers (1 mol eq, 0.400 mol) stirred continuously and heated to 80°C followed by the addition of re-crystallized pTSA (0.005 mol eq, 0.002 mol). DMP (0.83 mol eq, 0.334 mol) dissolved in acetonitrile was added dropwise to the monomer mixture and allowed to stir overnight. The crude polymer solution was concentrated under rotary evaporation, precipitated in cold ethanol, and vacuum dried. To further carry out hydroxyl functionalization, PTK dithiol polymers (1 mol eq, 0.060 mol) were dissolved in anhydrous tetrahydrofuran (THF) followed by the addition of $CsCO_3$ (5 mol eq, 0.15 mol) and 2-bromoethanol (5 mol eq, 0.15 mol) and allowed to react for 4 hours. The resulting PTK diol polymers was filtered, concentrated, precipitated in ethanol, and vacuum dried. Respective PTK diol polymers were dissolved in deuterated chloroform ($CDCl_3$) and their compositions were evaluated using 400 Hz ^{1}H nuclear magnetic resonance (NMR) spectroscopy (400 MHz Bruker); chemical shifts were reported as δ values in ppm relative to deuterated $CDCl_3$ (δ = 7.26).

EG0 (BDT) PTK diol; δ=1.60 (s, 6H, -S-C(C**H$_3$**)$_2$-S-), δ=1.65-1.69 (m, 4H, -S-CH$_2$-(C**H$_2$**)$_2$-CH$_2$-S-), δ=2.58-2.61 (t, 4H, -S-C**H$_2$**-(CH$_2$)$_2$-C**H$_2$**-S-), δ=2.69-2.73 (t, 2H, -S-C**H$_2$**-CH$_2$-OH), δ=3.68-3.72 (t, 2H, -S-CH$_2$-C**H$_2$**-OH).

EG1 (MEE) PTK diol; δ=1.60 (s, 6H, -S-C(C**H$_3$**)$_2$-S-), δ=2.72-2.76 (t, 2H, -S-C**H$_2$**-CH$_2$-OH), δ=2.78-2.82 (t, 4H, -S-C**H$_2$**-CH$_2$-O-CH$_2$-C**H$_2$**-S-), δ=3.58-3.64 (m, 4H, -S-CH$_2$-C**H$_2$**-O-C**H$_2$**-CH$_2$-S-), δ=3.68-3.74 (t, 2H, -S-CH$_2$-C**H$_2$**-OH).

EG2 (EDDT) PTK diol; δ=1.60 (s, 6H, -S-C(C**H$_3$**)$_2$-S-), δ=2.72-2.74 (t, 2H, -S-C**H$_2$**-CH$_2$-OH), δ=2.77-2.80 (t, 4H, -S-C**H$_2$**-[CH$_2$-O-CH$_2$]$_2$-C**H$_2$**-S-), δ=3.56-3.60 (m, 8H, -S-CH$_2$-[C**H$_2$**-O-C**H$_2$**]$_2$-CH$_2$-S-), δ=3.68-3.74 (t, 2H, -S-CH$_2$-C**H$_2$**-OH)

Synthesis of EG7 PTK diols

Synthesis of thioketal diethylamine was adapted from previously published work as shown in fig. S2 (*41*, *119*).

Mercaptoethyl trifluoroacetamide [1]. Cysteamine (1 mol eq, 0.47 mol) was dissolved in anhydrous methanol under nitrogen flow, followed by the addition of triethylamine (1.5 mol eq, 0.70 mol). Ethyl trifluoroacetate (1.2 mol eq, 0.56 mol) was added to the solution dropwise and allowed to stir on ice for 1 hour. The reaction mixture was brought to room temperature and stirred overnight. The concentrated reaction mixture was dissolved in water, extracted into ethyl acetate, dried over anhydrous magnesium sulfate, and concentrated in vacuo. The crude product was further purified by silica gel chromatography using a gradient of 100 to 70:30 ethyl acetate:hexane. The product (Compound [1], (fig. S2), a colorless liquid, was analyzed using 400Hz ^{1}H NMR; chemical shifts were reported as δ values in ppm relative to deuterated $CDCl_3$ (δ = 7.26) as follows; δ=2.7-2.76 (q, 2H, -NH-CH_2-C**H$_2$**-SH), 3.52-3.56 (t, 2H, -NH-C**H$_2$**-CH_2-SH), 7.01 (s, 1H, -N**H**-)

Thioketal diethyltrifloroacetamide [2]. Compound [1] (2.2 mol eq, 0.42 mol) was dissolved in acetonitrile and charged with N_2 gas followed by the addition of catalytic amounts of bismuth chloride ($BiCl_3$) (0.025 mol eq., 0.005 mol). DMP (1 mol eq., 0.192 mol) dissolved in acetonitrile was added to the flask dropwise and reaction was allowed to proceed at room temperature for 24 hours. Acetonitrile was removed from the mixture via rotary evaporation, and the crude product was filtered through silica in a mixture of 70:30 hexane:ethyl acetate for additional purification. The product (compound [2], (fig. S2), a white solid, was analyzed through 400Hz ^{1}H NMR in $CDCl_3$. Chemical shifts were reported as δ values in ppm relative to deuterated $CDCl_3$ (δ = 7.26) as follows; δ = 1.60 (s, 6H, -S-C(C**H$_3$**)$_2$-S-), 2.8-2.85 (t, 4H, -NH-CH_2-C**H$_2$**-S-), 3.56-3.61 (m, 4H, -NH-C**H$_2$**-CH_2-S-), 6.8 (s, 2H, -N**H**-)

Thioketal diethylamine [3]. Compound [2] (1 mol eq, 129 mol) was dissolved in minimal volume of methanol, and saponified in an aqueous 6M NaOH solution at room temperature for 4 hours. The resulting product was extracted into dichloromethane, dried over anhydrous magnesium sulfate, and concentrated under vacuum to obtain, a pale-yellow colored oil. Thioketal diamine crosslinker (Compound [3]) was then analyzed through 400Hz ^{1}H NMR in $CDCl_3$ (δ = 7.26) as follows; δ=1.53 (s, 6H) , -S-C(C**H$_3$**)$_2$-S-), 2.58-2.62 (t, 4H H_2N-CH_2-C**H$_2$**-S-), 2.66-2,69 (m, 4H, H_2N-C**H$_2$**-CH_2-S-)

PEG-NPC: Activated PEG 400 was synthesized as previously described (*120*). Briefly, PEG 400 (M_n = 400 Da) was dried at 80°C under vacuum for 24 hours. Dried PEG 400 (1 mol eq, 0.10 mol) was dissolved in anhydrous dichloromethane with triethylamine (1.2 mol eq., 0.12 mol) on ice. In a separate round bottom flask, p-nitrophenyl chloroformate (1.1 mol eq., 0.11 mol) was dissolved in anhydrous dichloromethane and added dropwise to the PEG400/triethylamine mixture. The reaction was mixed 30 minutes on ice and allowed to react for an additional 24 hours at room temperature. Triethylamine hydrochloride salts that were formed during the reaction were removed via filtration and the product was concentrated on a rotary

evaporator. This step yielded a mixture of monofunctionalized PEG nitrophenylcarbonate (OH-PEG-NPC) and homobifunctional PEG 400 dinitrophenylcarbonate (NPC-PEG-NPC).

The product was analyzed through 400Hz ^{1}H NMR in DMSO (δ = 2.5) as follows; δ = 3.5-3.6 (m, 28H, -[O-C**H$_2$**-C**H$_2$**]-), 3.71 (m, 2H, -O-C(=O)-O-CH$_2$-C**H$_2$**-O-), 4.4 (m, 2H, -O-C(=O)-O-C**H$_2$**-CH$_2$-O-), 7.6 (d, 2H, phenyl protons *meta* to nitro), 8.3 (d, 2H, phenyl protons *ortho* to nitro).

EG7 PTK diol. Activated PEG nitrophenylcarbonate mixture (OH-PEG-NPC/ NPC-PEG-NPC, 2.4 mol eq, 0.034 mol) dissolved in anhydrous dichloromethane was added dropwise to thioketal diamine crosslinker (Compound [3], 1 mol eq, 0.014 mol) and triethylamine (2.4 mol eq, 0.034 mol) which was allowed to react for 4 hours. The crude mixture was then precipitated in cold diethyl ether to remove p-nitrophenol impurities, and further purified through silica column chromatography. Crude product was loaded onto a silica packed column, and fractions of clean product were eluted using a mixture of dichloromethane and methanol at gradients of 0 to 10% methanol.

The fractions were then dried *in vacuo* and the product (50% yield) was analyzed through 400Hz ^{1}H NMR in DMSO (δ = 2.5) as follows; δ = 1.54 (s, 12H, -S-C(C**H$_3$**)$_2$-S-), 2.58-2.62 (t, 8H, C**H$_2$**-S-C(CH$_3$)$_2$-S-C**H$_2$**-), 3.11-3.16 (m, 8H, -S-CH$_2$-C**H$_2$**-NH-), 3.49-3.53 (m, 94H, -[O-C**H$_2$**-C**H$_2$**]-), 3.61 (t, 8H, O-C(=O)-O-CH$_2$-C**H$_2$**-O), 4.17 (t, 4H, O-C(=O)-O-C**H$_2$**-CH$_2$-O), 7.34 (s, 3H, -N**H**-).

Polyester polyol synthesis

Trifunctional polyester polyols (900t and 1500t) were synthesized as previously published (*121*). Briefly, glycerol was dried for 48 hours at 80°C under vacuum. Dried glycerol was added to a tri-neck flask, charged with nitrogen followed by the addition of 60% ε-caprolactone (CL), 30% glycolide (GA), and 10% D, L-lactide (LA) along with a stannous octoate catalyst to yield a 900Da triol and 1500Da triol.

Determination of molecular weight and hydroxyl number

Polymer molecular weights (M_n) and dispersities (Đ) were determined through dimethylformamide gel permeation chromatography (Agilent 1260 Infinity) with inline refractive index and light scattering detectors (Wyatt miniDAWN Treos), using Astra software and dn/dc values obtained from a refractometer (Anton Paar Abbemat 300). The hydroxyl (OH) number of the resultant polymeric diols was quantitatively determined via ^{19}F NMR spectroscopy using a method was adapted from Moghimi et al. (*122*). Briefly, 0.03 mmol of PTK diol was dissolved in deuterated acetone and reacted with 0.3 mmol of reagent 4-fluorophenyl isocyanate (4-F-Ph-NCO) for 15 mins at room temperature in the presence of 0.1 wt. % dibutyltin dilaurate (DBTDL) used as a catalyst and 0.081 mmol of α, α, α-trifluorotoluene (CF_3-Ph) as internal standard. The ^{19}F NMR spectrum in deuterated acetone was recorded as follows; δ= -63.23 (s, 3F,

CF_3-Ph), δ= -117.6 (m, 1F, 4-F-Ph-NCO), δ= -122.2 (s, 2F, 4-F-Ph-NH-CO-O-PTK). Theoretical hydroxyl number of each PTK diol was calculated by:

$$Mn = \frac{56{,}100 * f}{OH\#}$$

where 56,100 represents the molecular weight of KOH in mg/mol, *f* represents the hydroxyl functionality of the PTK (two for a linear homobifunctional PTK polymer) and M_n represents the number-average of the PTK polymers.

The logarithmic partition coefficient (LogP) of respective PTK diols were obtained computationally using the logP plugin for Marvin (ChemAxon). The octanol-water partition coefficient is commonly used to measure relative solubilities of a polymer.

Fourier transform infrared spectroscopy (FTIR) and differential scanning calorimetry (DSC)

10 uL of each PTK diol was applied in a thin layer between two 25 x 4 mm potassium bromide (KBr) glass windows and loaded into a Bruker Tensor 27 FTIR Spectrometer. Absorbance at 3400 cm^{-1} was used to identify OH groups for each PTK diol. In addition, absorbance peaks at 3330 cm^{-1} (N–H stretching) and 1630 cm^{-1} (carbonyl groups in urea bonds C=O) were identified to confirm the presence of NHCOO (urethane) bonds in EG7 PTK diols.

For glass transition temperature (T_g) analysis using differential scanning calorimetry (Q200, TA Instruments), samples ranging from 5 to 9 mg were heated from -80.0°C to 20.0°C at a rate of 10°C min^{-1}. Samples were then cooled to -80.0°C at a rate of 10°C min^{-1}, and heated a second time to 30°C at a rate of 10°C min^{-1}. All transitions were obtained from the second heating run.

Urethane foam fabrication

PTK and PE urethane (UR) scaffolds were fabricated using reactive liquid molding. Briefly, PTK-diols were mixed with calcium stearate (pore opener), TEGOAMIN33 (catalyst, Evonik), water (blowing agent), and sulfated castor oil (pore stabilizer) for 30 seconds at 3300 rpm in a Speed Mixer (Hauschild DAC 150 FVZ-L Speed Mixer (FlackTek, Inc., Landrum, SC). Lysine triisocyanate (LTI) was added and mixed for an additional 30 s at 3300 rpm. The mixture was allowed to rise, set, and harden overnight before the scaffolds were demolded and trimmed to shape. The target isocyanate: hydroxyl ratio (NCO OH) was set to 115:100 where the OH equivalents were obtained from polyol's molecular weight and OH number obtained from ^{19}F NMR analysis. The mass of each component for each scaffold formulation denoted as parts per hundred-part polyol (PPHP) was individually optimized and are outlined in table S2.

Urethane film synthesis and contact angle measurement

PE-UR and PTK-UR films (1mm thick) were synthesized by combining polymeric diols and bismuth neodecanoate (a gelling catalyst) in a 22 mm polyethylene mold for 30 seconds at 3300 rpm. LTI was then added to this mixture and mixed for additional 60 seconds. Urethane films were allowed to cure for 24 hours at room temperature before being demolded and punched into 4 mm circles using a biopsy punch.

Contact angle measurements were carried out using a goniometer (Rame-Hart, Model A-100). A 4µl water droplet was dispensed onto the surface of the urethane film and allowed to equilibrate for 10 mins. Bilateral contact angle measurements were obtained for each film, and averaged values across three different batches of urethane films were recorded for each formulation.

Sol fraction

Fabricated scaffolds were weighed to obtain the initial dry mass (M_o) and incubated in dichloromethane for 24 hours. Scaffolds were then removed from solvent, air dried and weighed to obtain the final mass (M_f). Soluble fraction (f_s) was calculated using the following equation:

$$f_s = \frac{M_o - M_f}{M_o} * 100$$

Swell ratio

To determine the swelling ratio of PTK-UR and PE-UR scaffolds, 10 mg (dry mass, M_d) scaffolds were incubated in phosphate-buffered saline (PBS) overnight and weighed to obtain swollen mass (M_s). The swell ratio was calculated using the following equation:

$$\%\, Swelling = \frac{M_s - M_d}{M_d} * 100$$

Dynamic mechanical analysis

Mechanical properties of PTK-UR and PE-UR scaffolds were measured in compression using the TA Q800 Dynamic Mechanical Analyzer. 6 x 6 mm cylindrical scaffold punches were hydrated in PBS for 24 hours prior to measurement. Scaffolds were longitudinally compressed under a preload force of 0.1N at 10% strain min^{-1} until 60% strain was reached. The longitudinal compression was repeated three times and values averaged per sample. The scaffolds were not rehydrated between these compression cycles. The Young's modulus for each sample was calculated from the linear region of the stress-strain curve after initial toe-in. A total of 3 scaffold pieces across three separate batches were averaged to obtain the Young's modulus of PU foams.

In vitro degradation of PTK-UR scaffolds

Pre-washed and dried 10 mg scaffold pieces (M_o) fabricated from PE or PTK diols were incubated in PBS and increasing concentrations of hydrogen peroxide/cobalt chloride ($H_2O_2/CoCl_2$) solutions to generate hydroxyl radical; 0.2% H_2O_2/0.001 M $CoCl_2$, 2% H_2O_2/0.01 M $CoCl_2$, or 20% H_2O_2/0.1 M $CoCl_2$. Scaffolds were incubated in 2 mL of treatment media for up to 30 days with media replaced every other day. At pre-determined time points, scaffolds were removed from the treatment media, rinsed in water, dried, and weighed to obtain the final remaining mass (M_t) of the scaffold. Three independent scaffold pieces were tested at each time point. Degradation was recorded as percent mass loss for each time point using the following equation:

$$\%\ Mass\ Remaining = \frac{M_t}{M_o} * 100$$

Mathematical modeling of PTK-UR scaffold degradation

MATLAB (MathWorks) was used to fit the oxidative degradation kinetics of PTK-UR scaffolds to a first order mathematical model based on H_2O_2 concentration using the following equation:

$$\frac{M_t}{M_o} = e^{-kt}$$

where M_t represents the final mass of scaffold time at time t, M_o represents the initial scaffold mass, and k represents the degradation rate constant. Non-linear regression was used to fit the experimentally obtained scaffold degradation data to the first order mathematical model to determine the degradation rate constant for each scaffold with respect to the degradation media concentration.

Scanning electron microscopy of urethane scaffolds

Scaffold pieces (60-80 mg) fabricated using PE and PTK diols were incubated in PBS or 2% H_2O_2 with 0.01M $CoCl_2$ for up to 15 days. At pre-determined intervals, scaffolds were removed from their respective treatments and washed in a series of graded ethanol solutions (30%, 50%, 70%, 80%,90%, 95% and 100%) for 10 minutes to remove the aqueous content of the degradation media. Scaffolds were then dried via critical point drying and weighed to obtain final scaffold mass. Dry scaffold pieces were then sputter coated (Cressington Scientific Instruments) with gold and imaged on a scanning electron microscope (Merlin, Carl Zeiss) using a Everhart-Thornley secondary electron detector at a beam voltage of 3.00 keV or 10 keV. Pore sizes from SEM images were quantified using ImageJ software.

DPPH radical scavenging assay

The radical scavenging potential of PE-UR and PTK-UR scaffolds were assessed using a 1,1-diphenyl-2-picrylhydrazyl (DPPH, Sigma Aldrich) assay (*123*). DPPH was dissolved in a mixture of 80:20 ethanol and H_2O (v/v%) at a concentration of 200 µM. Pre-fabricated PE and PTK urethane scaffolds (10 mg) were

treated with 2 mL of DPPH solution, and incubated at 37 °C on an orbital shaker for 36 hours. 100 µL of incubation solution was sampled at 1, 2, 3, 6, 12, 24, and 36 hour time points and the absorbance (A_{sample}) was measured at 517 nm and compared to control (no scaffold) DPPH solution absorbance ($A_{control}$). The scavenging potential is reported as following:

$$\% \, Inhibition = \frac{A_{Control} - A_{Sample}}{A_{Control}} * 100$$

ROS cell protection assay

Cell protection against cytotoxic levels of hydrogen peroxide was tested in NIH 3T3 fibroblasts. Briefly 10,000 cells were seeded in a 96 well plate in complete media (DMEM supplemented with 10% fetal bovine serum) and allowed to adhere overnight. Growth media was removed, and cells were sequentially treated with 100 µL of oxidative media (25 µM H_2O_2 or 50 µM H_2O_2) and 100 µL of test polyol solution and allowed to grow for an additional 24 hours. Post treatment, cell viability was assessed using CellTitre-Glo Luminescent Cell Viability Assay (Promega) and quantified by measuring bioluminescence on an IVIS 200 (PerkinElmer). Signal from treatment groups was normalized to untreated control cells and expressed as relative cell viability. The overall thioketal molar content (0.5 µmol) for each PTK diol test group was kept constant and control PE triol controls were formulated at 0.5 mg/mL to match the highest PTK diol mass.

Porcine excisional wound model and PTK-UR scaffold screening

All surgical procedures were reviewed and approved by Vanderbilt University Institutional Animal Care and Use Committee. Adolescent female Yorkshire pigs (n=3) were anesthetized with a cocktail of telazol (4.4 mg/kg), ketamine (2.2 mg/kg), and xylazine (2.2 mg/kg) administered intramuscularly and maintained under isoflurane for the duration of the surgery. Dorsal skin was shaved and disinfected using 70% ethanol, chlorohexidine, and betadine washes. Twenty-eight, full thickness 2 x 1 cm excisional wounds were created on the dorsum of the pig with two parallel rows of wounds produced on each side of the spine. Ethylene oxide-sterilized scaffold pieces were trimmed to 0.2 x 2 x 1 cm and implanted into the wounds after hemostasis was achieved. Each pig received all 5 treatments, placement was randomized to avoid anatomical bias. Following implantation of the test materials, wounds were covered with layerings of Mepilex Transfer (Molnlycke Healthcare), Mextra absorbent pad (Molnlycke), OpSite adhesive (Smith&Nephew), MediChoice Tubular Net Bandage (Owens & Minor), and Vetwrap (3M) bandaging. Following surgery, dressings were changed every 2-3 days under anesthesia. Antibiotics (Excede; Zoetis) were administered weekly during the study period. Buprenex was given immediately post-surgery, and analgesia was maintained for 7 days post-op using a transdermal Fentanyl patch (50 mcg/h) applied at the time of surgery and changed every 2-3 days. In independent studies, animals were euthanized at either 10 or 24 days post-surgery; wound samples were collected in anesthetized pigs using 2 mm biopsy punches

for gene expression analysis. Post euthanasia, the remaining wound site was excised with in the wide margins for histological analyses.

Porcine testing of PTK-UR against clinical controls

Integra Bilayer Wound Matrix (BWM) (Integra Life Sciences) was rinsed in sterile saline, trimmed to 2 x 1 cm pieces, and placed matrix side down into the excisional bed. The protective silicone layer was removed 14 days post application, according to manufacturer's guidance. NovoSorb Biodegradable Temporizing Matrix (BTM) (PolyNovo) scaffolds were trimmed to 2 x 1 cm pieces and applied matrix side down into the full thickness skin wound. Sealing polyurethane membrane was removed 21 days post application according to manufacturer's guidance. EG7 PTK-UR scaffolds were similarly applied. Treatments were randomized with regards to wound location to avoid any anatomical bias. The wounds were dressed and secured with additional bandaging as described above. Pigs were euthanized 31 days post-surgery and wound samples were collected for histology and gene expression analysis as previously described.

Testing PTK-UR and NovoSorb Dermal Matrices in a Porcine Ischemic Wound Model

Under sterile conditions, four pairs of full thickness incisions 15 cm in length and 10 cm wide were created parallel to the spine (two cephalic and two caudal), as previously described (*35*). Using a cautery, the skin was lifted from the underlying fascia to create bipedicle flaps. The resulting flaps of skin were re-approximated with staples creating four distinct ischemic regions on the dorsal region of the pig (n=1). Two laterally symmetrical 1 cm^2 full-thickness excisional wounds were then created within each of the four ischemic flaps. 1 x 1 cm^2 sized EG7 PTK-UR and NovoSorb BTM scaffolds were implanted into the skin wounds. Each flap received one of each scaffold type, and treatments locations were otherwise randomized to prevent anatomical bias. The wounds were dressed as described above for non-ischemic wounds. The dressings were changed every 3 days. The protective membrane overlayer present on NovoSorb BTM was removed 14 days post application. The pig was euthanized 17 days post-surgery, and wound samples were collected for histological analysis.

Laser doppler perfusion imaging

A laser doppler imager (moorLDI2-HIR; Moor Instruments) was used to track blood perfusion within the wounds over the duration of the study. Flux images of wounds were obtained after scaffold implantation and subsequently during dressing changes at days 1, 4, 10, 17, 24, and 31 post-surgery. Blood perfusion within a 2 x 1 cm region of interest as well as adjacent uninjured skin was quantified using Moor analysis software. Data are presented as total flux within the wounds, normalized to the total flux recorded in normal skin.

Blood perfusion within ischemic wounds was also measured using doppler imaging, with data acquired at days 1, 3, 5, 7, 9, 11, 14 and 17 post-surgery. Blood perfusion was quantified within the wound area and presented as total flux.

Histology and quantification

Tissue samples were fixed in 10% neutral buffered formalin for 48 hours and were then dehydrated in a graded ethanol series, exposed to xylene, and embedded in paraffin. Tissue sections (5μm thick) were deparaffinized in gradients of xylene and ethanol and rehydrated in Tris-Buffered Saline/0.1% Tween 20 (TBST) buffer. Masson's trichrome staining and hematoxylin and eosin (H&E) staining were performed according to the manufacturer's recommendation. Antigen retrieval was performed using citrate-based pH 6 antigen retrieval solution (Dako) for 1 minute at 120°C and allowed to cool to 90°C. Sections were then incubated for 40 minutes in 3% H_2O_2 TBST solution and blocked with protein block (Dako) for 20 minutes. Sections were further incubated in either rabbit anti-human von Willebrand factor (GA52761-2, Dako), mouse anti-human cytokeratin14 (MCA890, Biorad), mouse anti-αSMA (A2547, Sigma Aldrich), rabbit anti-CCR7 (ab32527, abcam), rabbit anti-arginase-1 (ab91279, abcam), rabbit anti-CD3 (ab16669, abcam), rabbit anti-human myeloperoxidase (A039829-2, Dako), or rabbit anti-CD206 (18704.1. AP, Proteintech), mouse anti-9-hydroxy-2'-deoxyguanosine (ab48508) for 60 minutes at room temperature. Secondary antibodies donkey anti-mouse HRP (Envision+/HRP, Dako) or donkey anti-rabbit HRP (Envision+/HRP, Dako) were applied for 30 minutes at room temperature followed by 3,3′-diaminobenzidine (DAB) substrate (Dako) for 5 minutes. Slides were then rinsed in TBST buffer, dehydrated in graded ethanol and xylene solutions, and mounted with Acrytol (manufacturer) mounting media.

Histological sections were imaged and evaluated using Metamorph Imaging Software (Molecular Devices) and ImageJ to assess wound thickness occupied by scaffold and tissue infiltration within the scaffold pores. Wound thickness occupied by scaffold was defined as the longitudinal thickness of the granulation tissue occupied by the bulk scaffold/scaffold remnants. Tissue infiltration was defined as percent area occupied by new granulation tissue within the scaffold pores, averaged across 3 fields of view per sample. Using Metamorph imaging software, Brown pixels (positive immunoreactivity for DAB) were quantified for each IHC marker (CytoK14, CD206, MPO, CD3 and vWF). Epithelialization was quantified as percent wound length covered by K14-positive epidermal layer. vWF, MPO, CD206, and CD3 were quantified and expressed as percent region of interest (ROI) area occupied by positive brown pixels. A minimum of three fields of view per wound sample were analyzed and quantified. Using ImageJ, analysis of CCR7 IHC was performed on color deconvolved (Image J Plugin) DAB-hematoxylin images. Plot intensity measurement on DAB isolated images were performed up to 150 μm from the edge of the scaffold to obtain measurements for CCR7 staining intensity.

Wound Scoring

Treatment-blinded histomorphometric analysis of trichrome- and H&E-stained tissue sections was used for histological scoring of wounds based on a composite evaluation of five parameters: extent of granulation tissue formation (G), degree of vascularization (V), re-epithelialization (E), collagen deposition (amount and fiber orientation) (C), and inflammation (I) as shown in table S1. A serial section stained with trichrome stain was scored to estimate the extent of and organization of new connective tissue. Each parameter was rated on a 1-5 scale, ranging from little or no activity to near-complete reorganization of tissue. The overall score comprised of G+V+E+C-(I/2) was assigned to each wound with a higher score indicating a more favorable wound healing response. Semi-quantitative analysis for the formation of foreign body giant cells (FBGC) was performed on the group of wounds treated with EG7 PTK-UR, NovoSorb, and Integra. The foreign body response was scored by evaluation of hematoxylin and eosin-stained tissue sections. A score of 0 indicated little or no association of FBGC with residual scaffold fragments, and a score of 5 represented intense association of both mononuclear cells and FBGC with persistent scaffold material. In the current series, the maximum FBGC reaction score was 3. In this experiment, an additional FBGC score between 1-5 was assigned to each wound and subtracted from the total wound healing score to account for foreign body response to the implanted materials.

Gene expression analysis of granulation tissue

Wound samples were excised at predetermined time points and stored in RNA*later* Stabilizing Solution (Invitrogen) at -20°C. Total RNA was extracted from tissue using QIAzol Lysis Reagent (Qiagen). Briefly, tissue samples were minced and homogenized in QIAzol using a Tissue Lyser (Qiagen). Tissue homogenate was phase separated using chloroform, and the aqueous RNA layer was collected and processed using a RNeasy Mini kit (Qiagen) to eliminate phenolic impurities carried over from QIAzol extraction. During the column-based cleanup process, on-column DNase treatment was performed to eliminate genomic DNA from the samples. RNA samples were reverse transcribed to cDNA and quantified using a custom porcine Qiagen PCR Array Kit. Genes involved in various wound healing phases including inflammatory cytokines and interleukins, transcription factors, cell surface markers, ECM components, growth factors and remodeling enzymes were included in the panel.

Mouse subcutaneous scaffold implantation

All surgical procedures were approved by the Vanderbilt University Institutional Animal Care and Use Committee. The ventral region of C57BL/6 mice was shaved and prepped with betadine and ethanol, followed by the creation of small incisions, one on either side of the midline. The incisions allowed for the dissection of subcutaneous pockets for scaffold implantation. EG2 PTK-UR and EG7 PTK-UR scaffolds

were trimmed to 6 x 1 mm discs, UV sterilized, and implanted in the subcutaneous pockets that were then sutured close to secure the scaffolds in place. Each mouse received 2 scaffolds of the same formulation. Mice were similarly implanted with 900t PE-UR and EG7 PTK-UR scaffolds to assess relative ROS expression associated with each scaffold chemistry in vivo.

Assessment of H_2O_2 levels in mice using Amplex Red

Mice were euthanized 4 days post-implant to retrieve scaffolds from the subcutaneous space. The explanted scaffolds were weighed, minced, and incubated in 0.5 mL of the Amplex Red reaction mixture (prepared according to kit instructions) for 1 hour at room temperature. Following incubation, the fluorescence intensity of the sample supernatants were measured, and the average fluorescence measures from each sample was normalized to the scaffold mass.

Mouse scaffold retrieval and cell isolation

Mice were euthanized 7, 14, and 21 days post-surgery to retrieve scaffolds from the subcutaneous sites. Cells from two scaffolds of the same formulation, implanted in the same mice were pooled for analysis. Scaffolds from each mouse were finely minced in 1 mL PBS and the resultant tissue slurry was digested in a solution of Collagenase D (2 mg/mL, Sigma Aldrich), DNase1 (0.1 mg/mL, Sigma Aldrich), and Liberase TL (0.7 mg/mL, Sigma Aldrich) for 30 minutes at 37 °C on an orbital shaker. The digested cell solution was filtered through a 100 µm cell strainer to removed undigested tissue, treated with ACK lysis buffer (ThermoFisher Scientific) to remove red blood cells, and washed with cold PBS supplemented with 2 mM EDTA and 1% FBS. The cell suspension was pelleted and resuspended at $2x10^{\wedge 6}$ cells/mL. 250 µL of the cell suspension was transferred into polystyrene tubes for antibody staining for each of the two panels.

Flow cytometry

The suspended cells from each treatment and time point were blocked with Fc block (Invitrogen) for 5 mins and stained for myeloid cell surface markers using the following antibody panel: DAPI, CD45 BriliantViolet 510, F4/80 FITC, CD206 PE, CD11c PerCP-Cy5.5, CD86 PE-Cy7, CD301b eFluor660, and CD11b APC-Cy7 (fig. S11B) for 30 minutes at 4°C. Cells were then washed with 1% FBS in PBS before analysis. All cell populations were gated on live immune cells (DAPI/CD45) prior to phenotype specific gating.

For the lymphoid analysis, cells were stained with Live/DEAD Fixable dye (Invitrogen) followed by a solution of surface markers for 30 minutes at 4°C including CD45 BriliantViolet 510, CD8a FITC, TCRγδ PE-Cy7, CD4 APC, and TCRβ APC-Cy7. After staining for surface markers, cells were fixed with True Nuclear Transcription Factor Staining Kit (Biolegend) for 60 minutes at room temperature and stained for FOXP3 PE and GATA3 PerCP-Cy5.5 intracellular markers for an additional 30 minutes. Cells were washed

with 1% FBS in PBS before being analyzed. All cell populations were gated on live immune cells (Viability dye/CD45) prior to phenotypic specific gating.

Gates (fig. S11A) were set using fluorescence minus one (FMO) and positive controls. Leukocytes were defined as live $CD45^+$ cells; monocytes and neutrophils were defined as $CD45^+CD11b^+F4/80^-$ population. The $CD45^+CD11b^+F4/80^+$ population (pan macrophage population) was further analyzed for the presence of CD206 surface marker and the $CD45^+CD11b^+F4/80^+CD206^+$ population was isolated. Presence of CD301b surface marker within the $CD45^+CD11b^+F4/80^+CD206^+$ macrophage population was quantified and presented as mean fluorescence intensity (MFI) adapted from Shook et al. (*67*). Within the $CD45^+CD11b^+F4/80^+$ macrophage population, we further analyzed the expression of CD11c surface markers and isolated two population, $CD45^+CD11b^+CD11c^+F4/80^+$ ($CD11c^+$ macrophage) and $CD45^+CD11b^+CD11c^-F4/80^+$ ($CD11c^-$ macrophage population); dendritic (DCs) cells were characterized as $CD45^+CD11c^+F4/80^-$. Lymphocytes were separated into $TCR\beta^+TCR\gamma\delta^-$ and $TCR\beta^-TCR\gamma\delta^+$ to define two lymphoid populations. $TCR\beta^+TCR\gamma\delta^-$ were further divided into $CD8a^+CD4^-$ and $CD8a^-CD4^+$ populations to identify cytotoxic T lymphocytes (CTLs) and helper T (T_H) cells respectively. The $CD8a^-CD4^+$ T helper cell population was used to identify $FoxP3^+$ and $GATA3^+$ regulatory T cells and type 2 helper T cells (T_H2). All analyses were performed in FlowJo Flowcytometry Analysis Software (Treetar)

Supplementary Figs

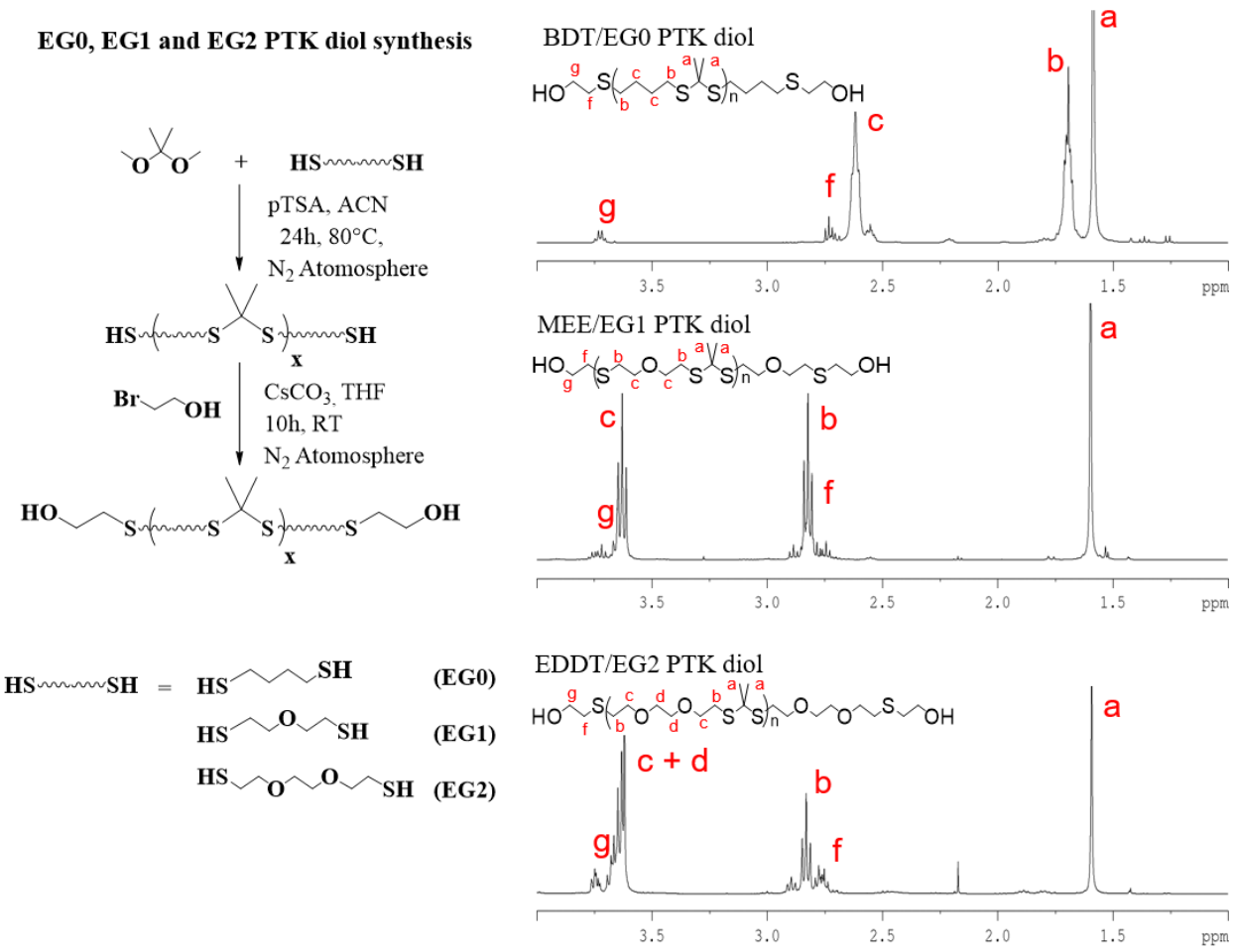

Fig. S1. Synthesis and ^{1}H NMR characterization of EG0, EG1 and EG2 PTK diols. Synthesis scheme for condensation polymerization of BDT (EG0), MEE (EG1) and EDDT (EG2) dithiol monomers to obtain PTK dithiol polymers and their functionalization with bromoethanol to synthesize PTK diol polymer. On the right, ^{1}H NMR spectra of BDT PTK diol, MEE PTK diol and EDDT PTK diol showing accurate chemical composition.

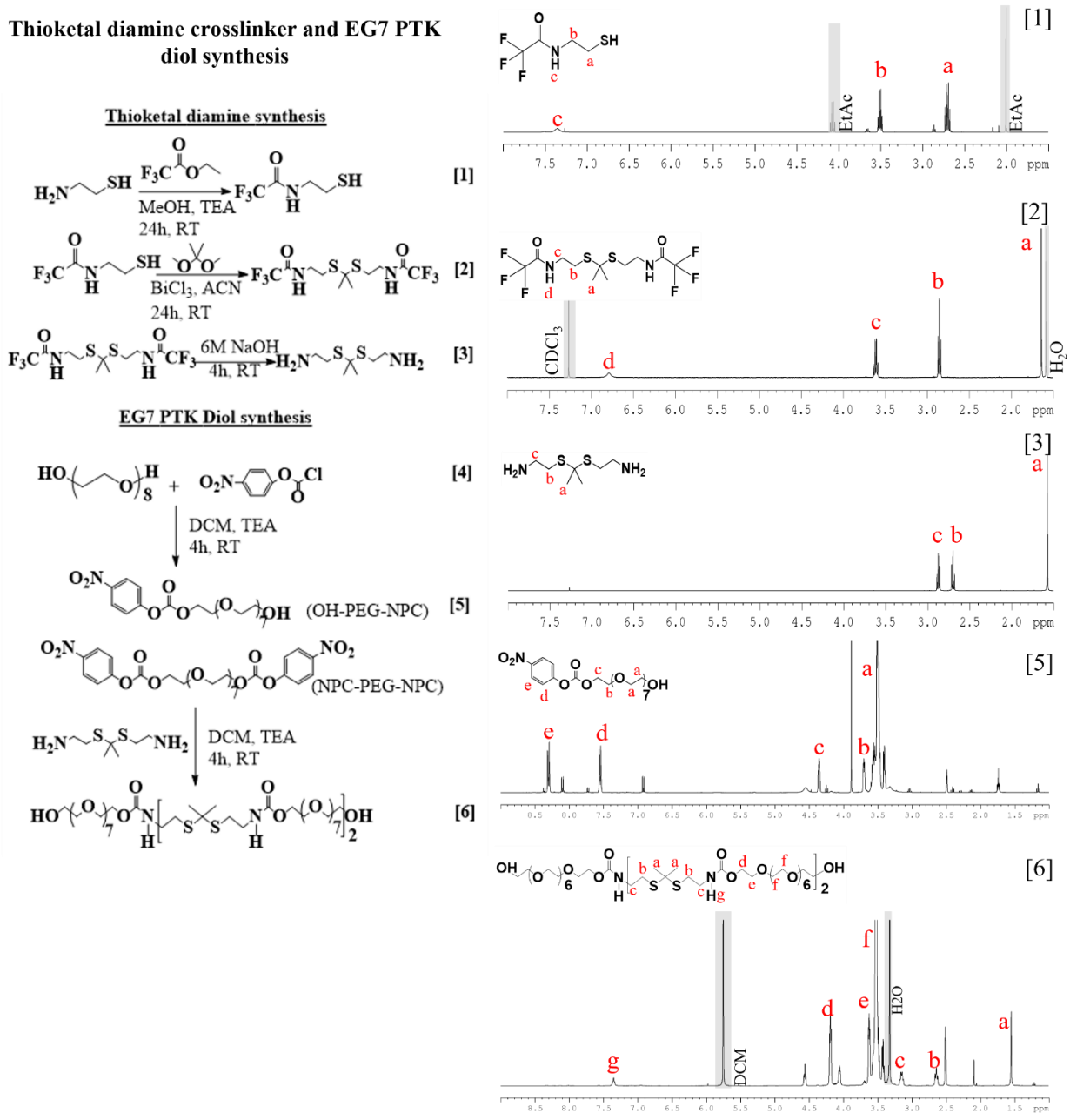

Fig. S2. Synthesis and ^{1}H NMR characterization of EG7 PTK diol. ROS-degradable thioketal (TK) diamine crosslinker and EG7 PTK diol through the reaction of TK diamine and amine reactive OH-PEG-NPC/NPC-PEG-NPC. On the right, ^{1}H-NMR spectroscopy of compounds 1, 2, 3, 5 and 6 are shown.

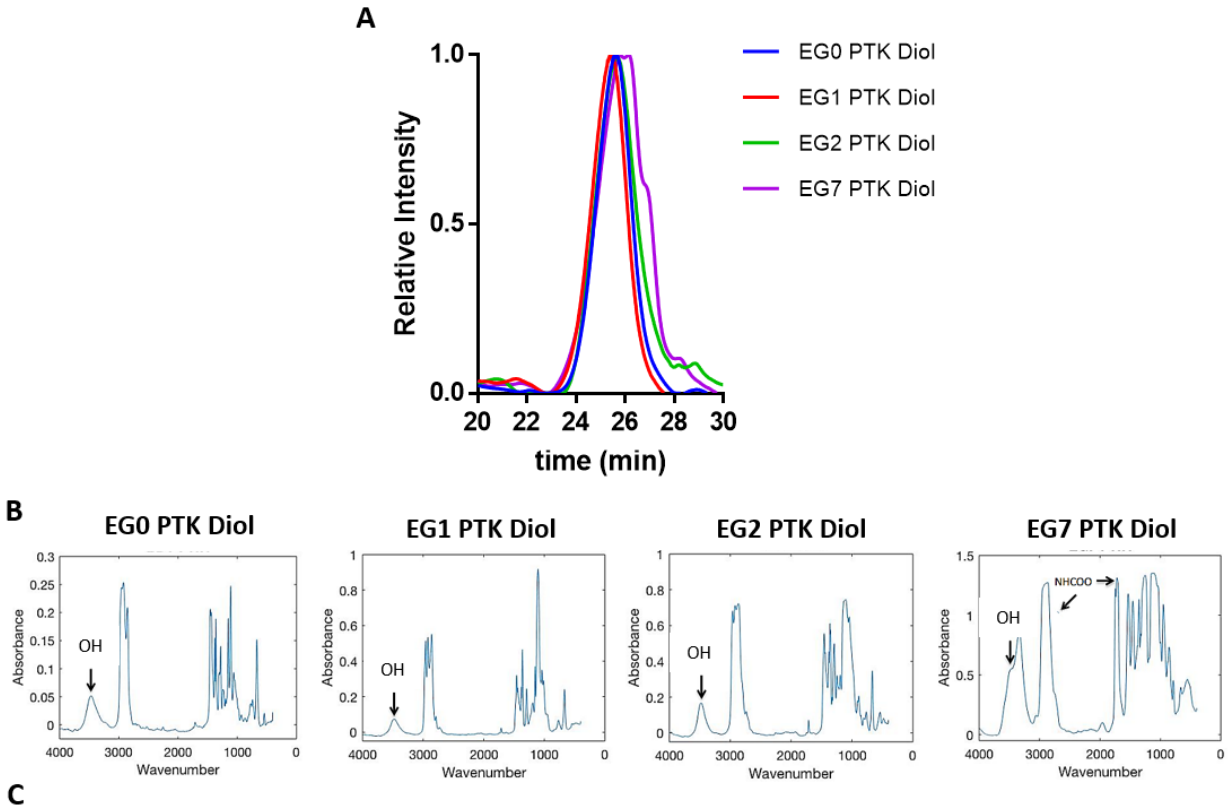

C

PTK diol	M_n	dn/dc	Dispersity	RU	OH # Theoretical	OH # Calculated	Tg (°C)
EG0 PTK diol	2100	0.1100	1.10	11.7	53	49	-56.29
EG1 PTK diol	2200	0.1084	1.10	10.2	51	53	-56.57
EG2 PTK diol	2100	0.1055	1.15	8.2	53	51	-62.09
EG7 PTK diol	1500	0.0663	1.20	1-2	75	63	-48.09

Fig. S3. Characterization of PTK diols. (**A**) GPC elutograms for EG0, EG1, EG2, and EG7 polymers. (**B**) FTIR spectra of hydroxyl terminated poly(thioketal) (PTK) polymers with hydroxyl absorbance peak seen at 3400 cm-1 (black arrow). (**C**) Table showing number average molecular weight (M_n), dispersity index, thioketal repeating unit (RU), hydroxyl number (OH#, calculated through ^{19}F NMR), and glass transition temperate (T_g) of EG0, EG1, EG2, and EG7 PTK diols.

A

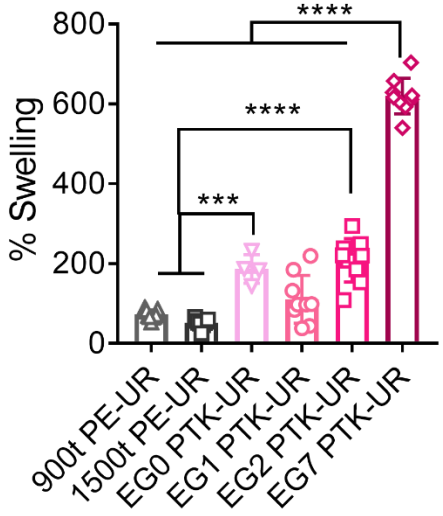

B

	Sol Fraction (%)	Core Porosity (%)	Pore Size (μm)
900t PE-UR	1.71 ± 1.11	87.05 ± 1.27	92.4 ± 20.1
1500t PE-UR	4.18 ± 3.51	87.53 ± 2.43	74.2 ± 24.2
EG0 PTK-UR	4.16 ± 1.31	89.45 ± 2.85	91.7 ± 49.9
EG1 PTK-UR	1.13 ± 0.23	86.80 ± 1.66	106.6 ± 45.1
EG2 PTK-UR	5.42 ± 2.01	88.60 ± 1.81	133.3± 23.0
EG7 PTK-UR	15.02 ± 2.58	91.48 ± 0.03	132.6± 30.0

Fig. S4. **Characterization of PE-UR and PTK-UR scaffolds.** (**A**) Swell ratio of PE and PTK based urethane foams hydrated in PBS, (**B**) Physical properties of PE-UR and PTK-UR scaffolds. Data is presented as Mean ± SD. ***$P < 0.001$, ****$P < 0.0001$ by analysis of variance (ANOVA).

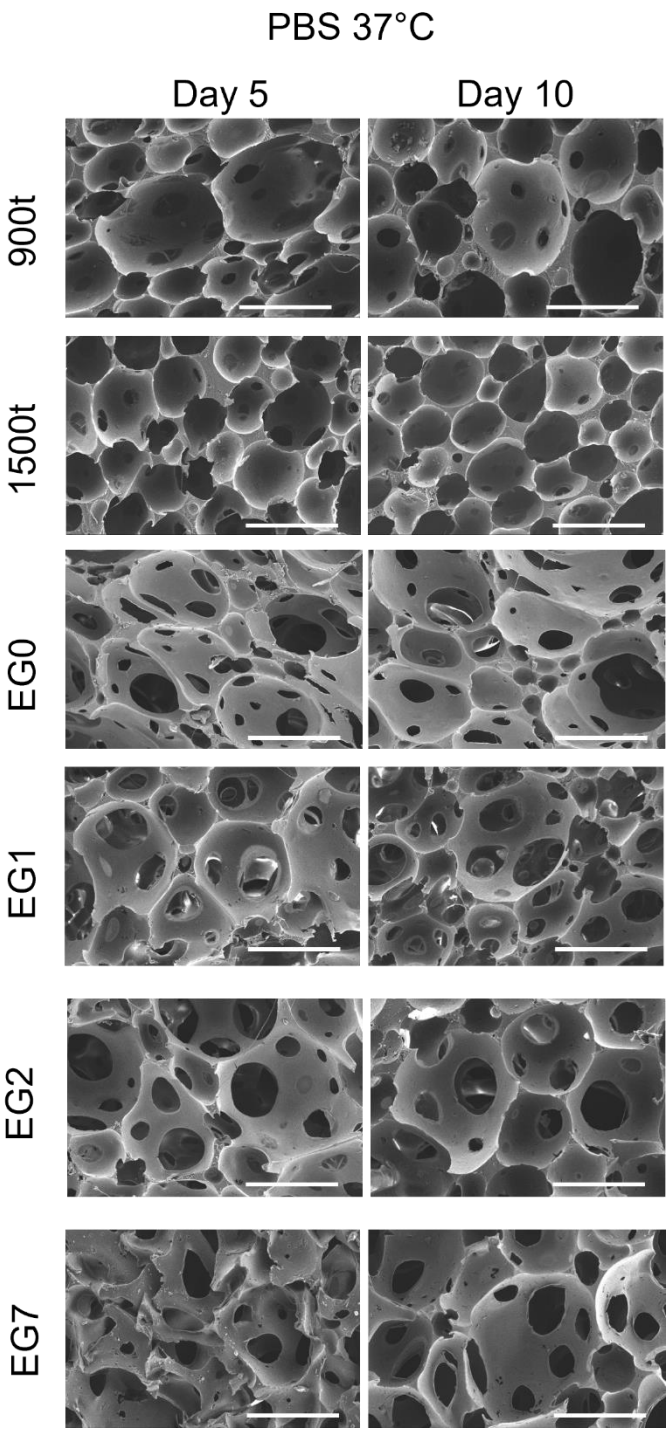

Fig. S5. Hydrolytic degradation of PU scaffolds in vitro. Representative SEM images of in vitro PTK and PE-UR scaffold degradation incubated in hydrolytic media (PBS) for 15 days. Scale bar = 200 μm.

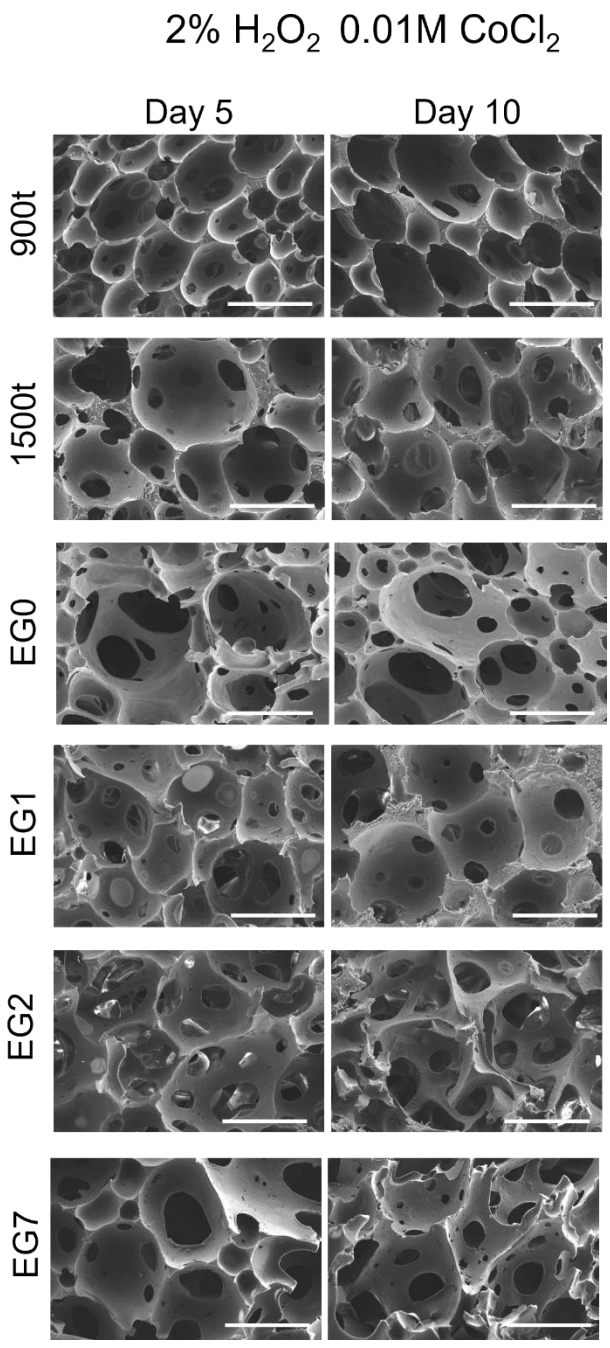

Fig. S6. Oxidative degradation of PU scaffolds in vitro. Representative SEM images of in vitro PTK and PE-UR scaffold degradation incubated in oxidative media simulated by 2% H_2O_2 0.01M $CoCl_2$ for 15 days. Scale bar = 200 μm.

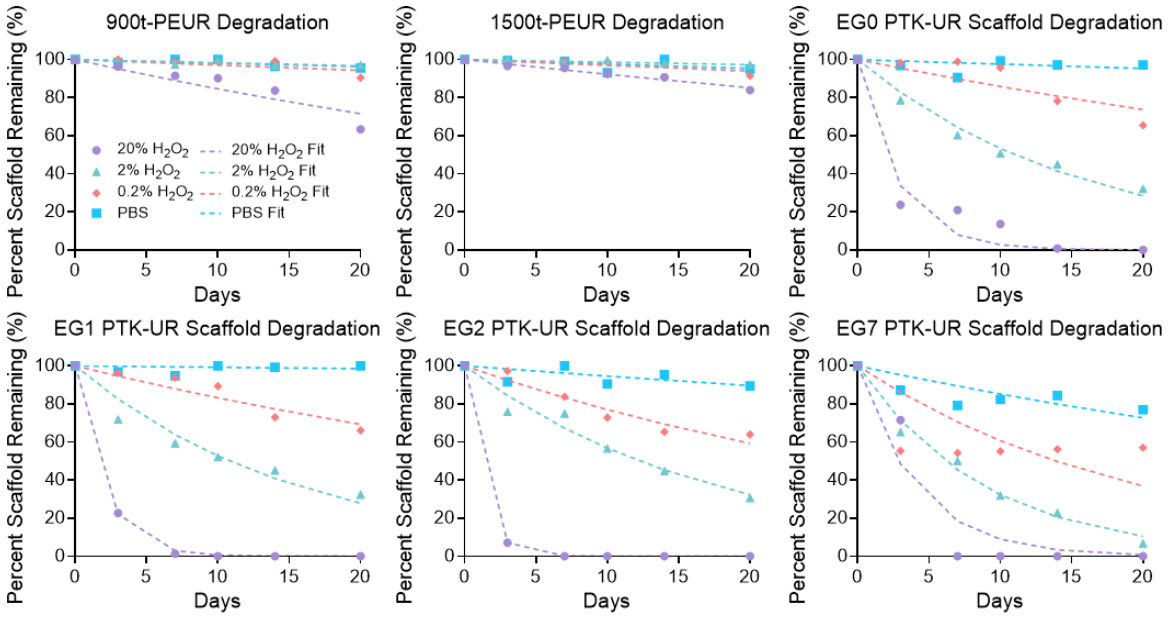

Fig. S7. In vitro degradation kinetics of PU scaffolds. Graphs show dose dependent degradation in oxidative media and relative stability in hydrolytic media over 30 days. Dashed lines represent MATLAB model-generated curves for degradation kinetics.

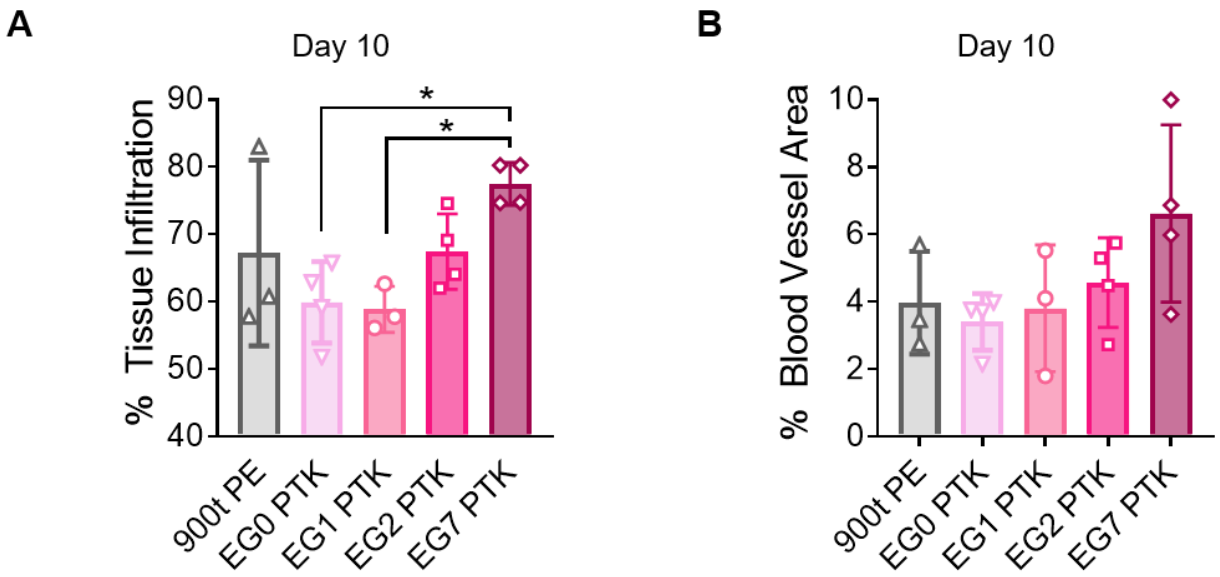

Fig. S8. Characterization of porcine skin wounds treated with PU scaffolds. Quantification of (**A**) tissue infiltration and (**B**) blood vessel area within scaffold infiltrating tissue 10 days post-wounding of porcine skin. Data presented as Mean ± SD, n = 3-4 wounds. Data presented as Mean ± SD. **P* < 0.05 by ANOVA.

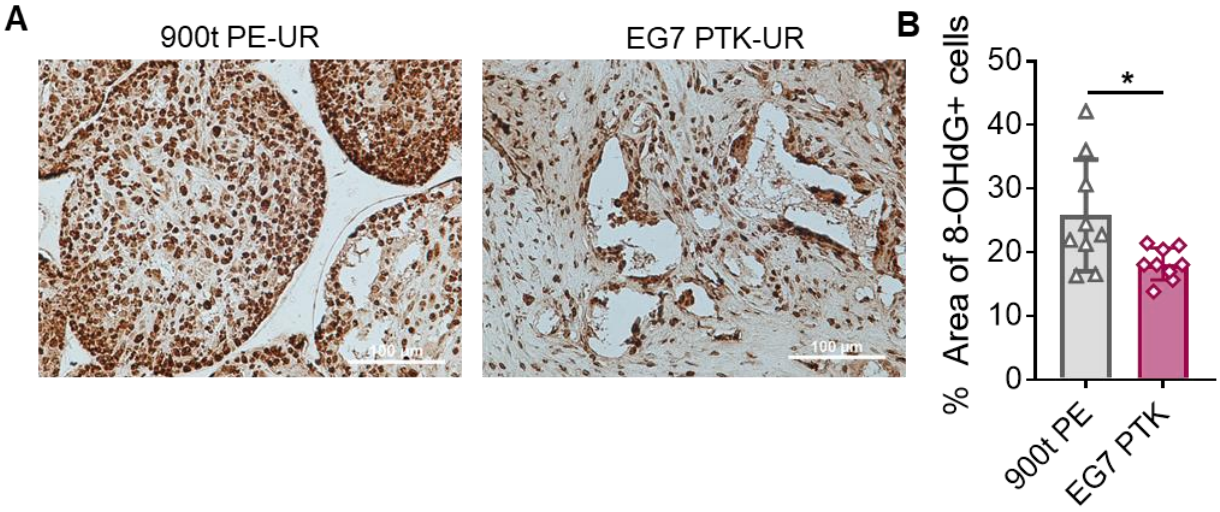

Fig. S9. Oxidative stress in PE-UR and EG7 PTK-UR treated porcine skin wounds. (**A**) 8-OHdG IHC of PE-UR and EG7 PTK-UR treated day 10 porcine wounds. (**B**) DNA oxidation products in wounds treated with PTK-UR scaffolds compared to PE-UR. Mean ± SD, n = 9 high powered fields acquired from 2-3 wounds per scaffold type. Data presented as Mean ± SD. **P* < 0.05 by Welch's t-test.

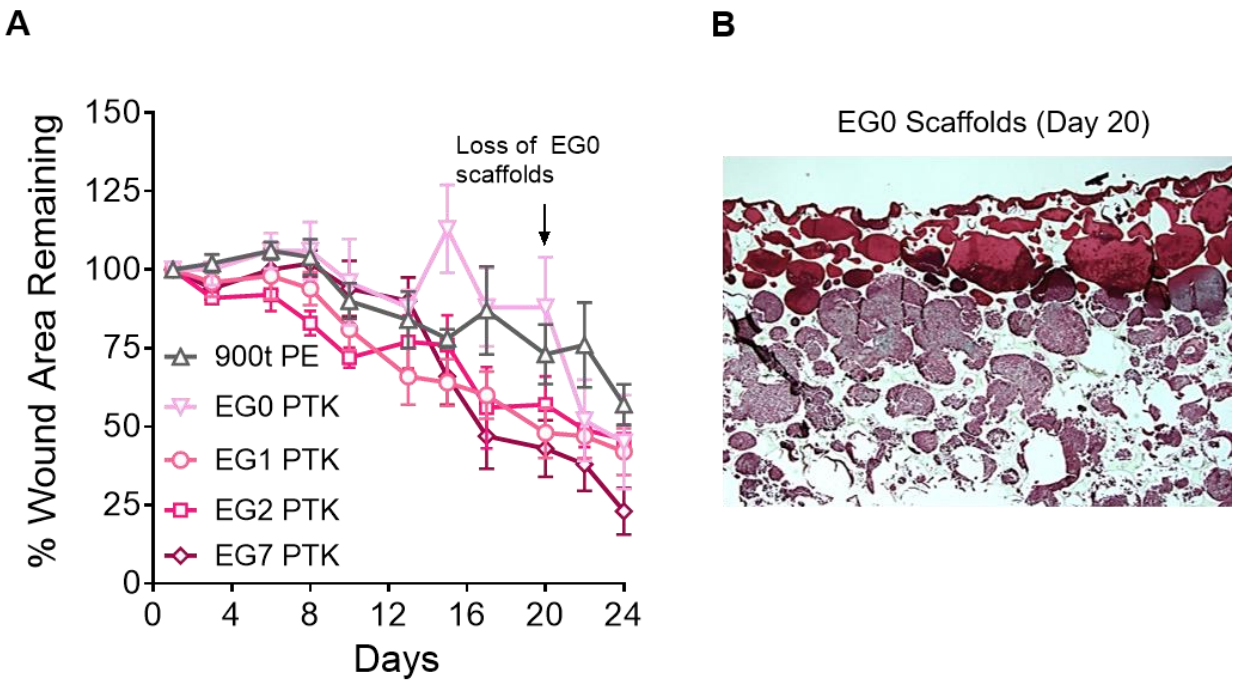

Fig. S10. Wound closure of PU scaffold treated porcine skin wounds. (**A**) Quantification of porcine skin wound area remaining open over a period of 24 days of scaffold-treated porcine skin wounds. (**B**) Representative trichrome image showing tissue infiltration within EG0 PTK-UR scaffold pores 20 days post implantation. Scaffolds were extruded from the wound post application. Data presented as Mean ± SD (n = 3-4 wounds per group).

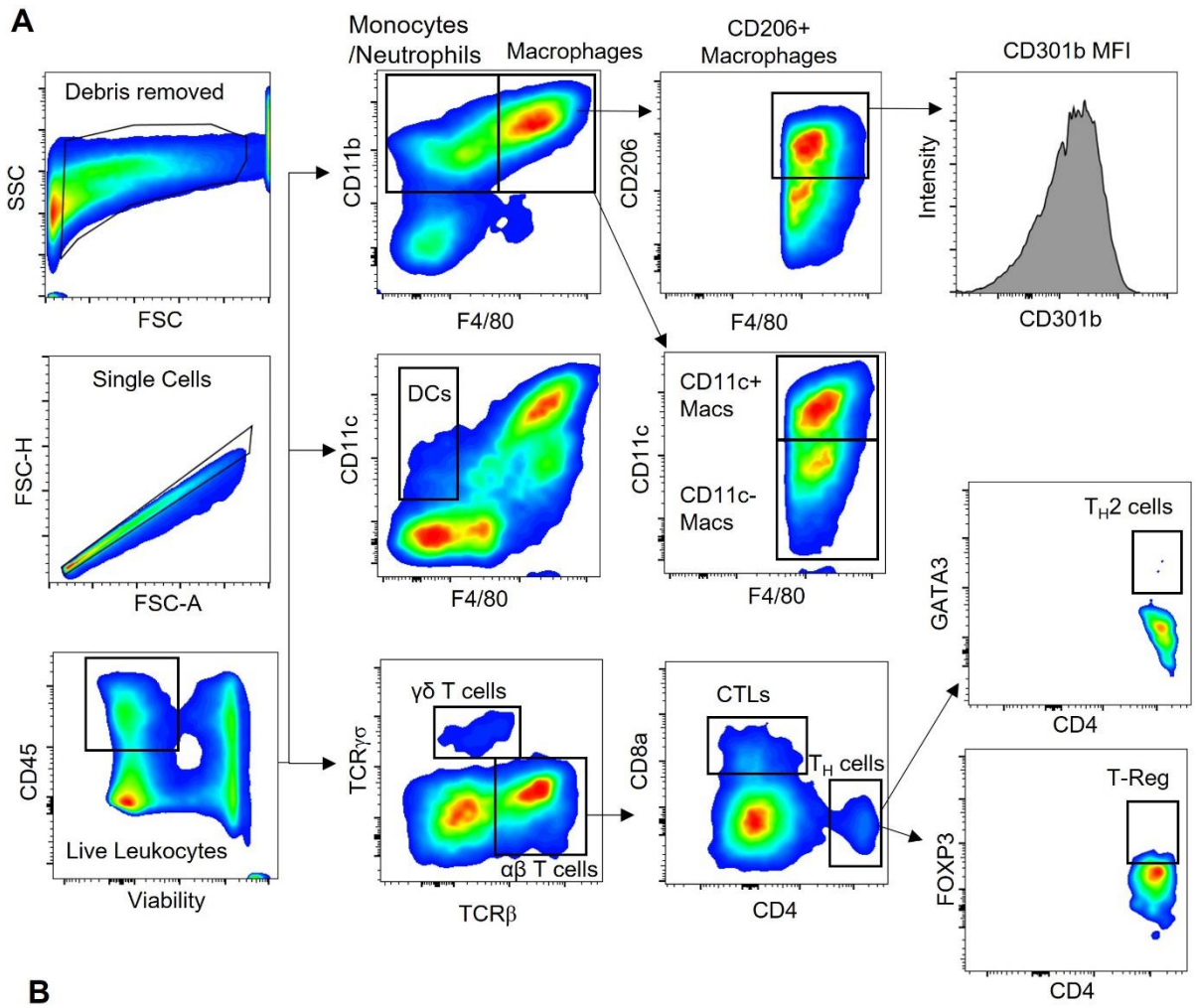

B

Antigen	Clone	Fluorophore	Cat#
Viability	-	DAPI	
CD45	30-F11	BV510	Biolegend 103138
F4/80	BM8	FITC	Biolegend 123107
CD206	C068C2	PE	Biolegend 141706
CD11c	N418	PerCP-Cy5.5	Biolegend 117327
CD86	GL1	PE-Cy7	eBioscience 25-0862-82
CD301b	11A10-B7	eFluor660	eBioscience 50-3011-82
CD11b	M1/70	APC-Cy7	Biolegend 101226

Antigen	Clone	Fluorophore	Cat#
Viability	-	Violet Live Dead	Molecular probes (L34955)
CD45	30-F11	BV510	Biolegend 103138
CD8a	53-6.7	FITC	Biolegend 100706
FOXP3	MF23	PE	BDPharmingen 560408
TCRγδ	GL3	PerCP-Cy5.5	Biolegend 653811
GATA3	TWAJ	PE-Cy7	eBioscience 25-5711-80
CD4	RM4.5	APC	Biolgend 100516
TCRβ	H57-597	APC-Cy7	Biolegend 109220

Fig. S11. Flow cytometry strategies to isolate immune subtypes. (**A**) Gating strategies for myeloid and lymphoid populations. Cells were gated on SSC and FSC, followed by doublet discrimination to isolate the single cell population based of FSC-A and FSC-H. Cells were gated on live immune cells (DAPI+CD45+) or (Viability dye+CD45+) prior to phenotypic specific gating (**B**) Tables of antibody clones used in flow cytometry and immunophenotyping of myeloid and lymphoid cells.

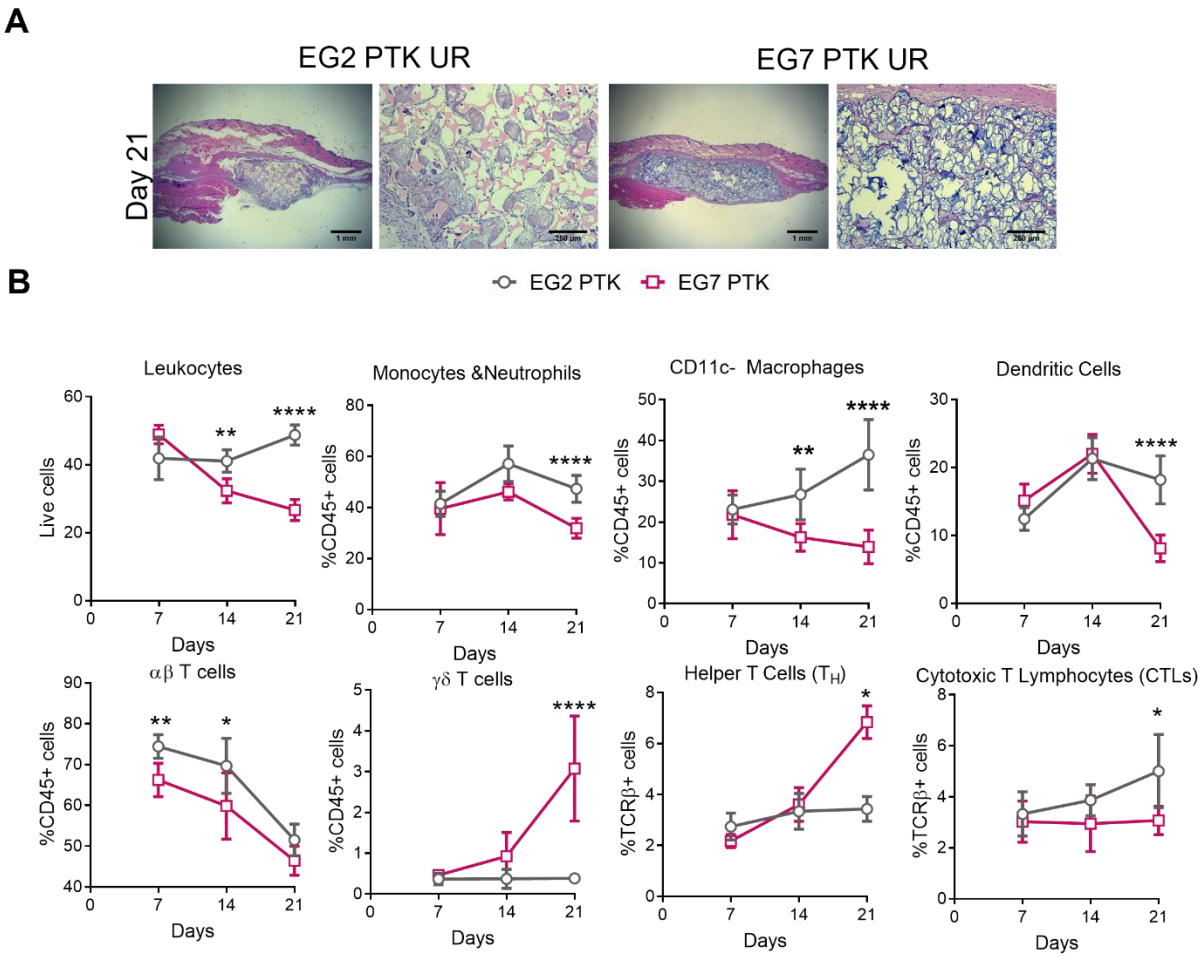

Fig. S12. Analysis of infiltrating immune cell populations within EG2 and EG7 PTK UR scaffolds implanted in mice. (**A**) 6 mm x 1.5 mm EG2 and EG7 PTK-UR scaffolds implanted in subcutaneous pockets of C57BL/6 mice and explanted after 21 days. Representative H&E images showing tissue infiltration and immune cell recruitment into scaffold pores (high mag, scale bar = 1 mm and low mag, scale bar = 250 µm). (**B**) Change in leukocyte sub-populations in EG2 PTK (gray) and EG7 PTK (pink) cellular infiltrates measured 7, 14 and 21-days post implantation. Data presented as Mean ± SD, n = 6 mice, * $P < 0.05$, ** $P < 0.01$, **** $P < 0.0001$ by analysis of variance (ANOVA).

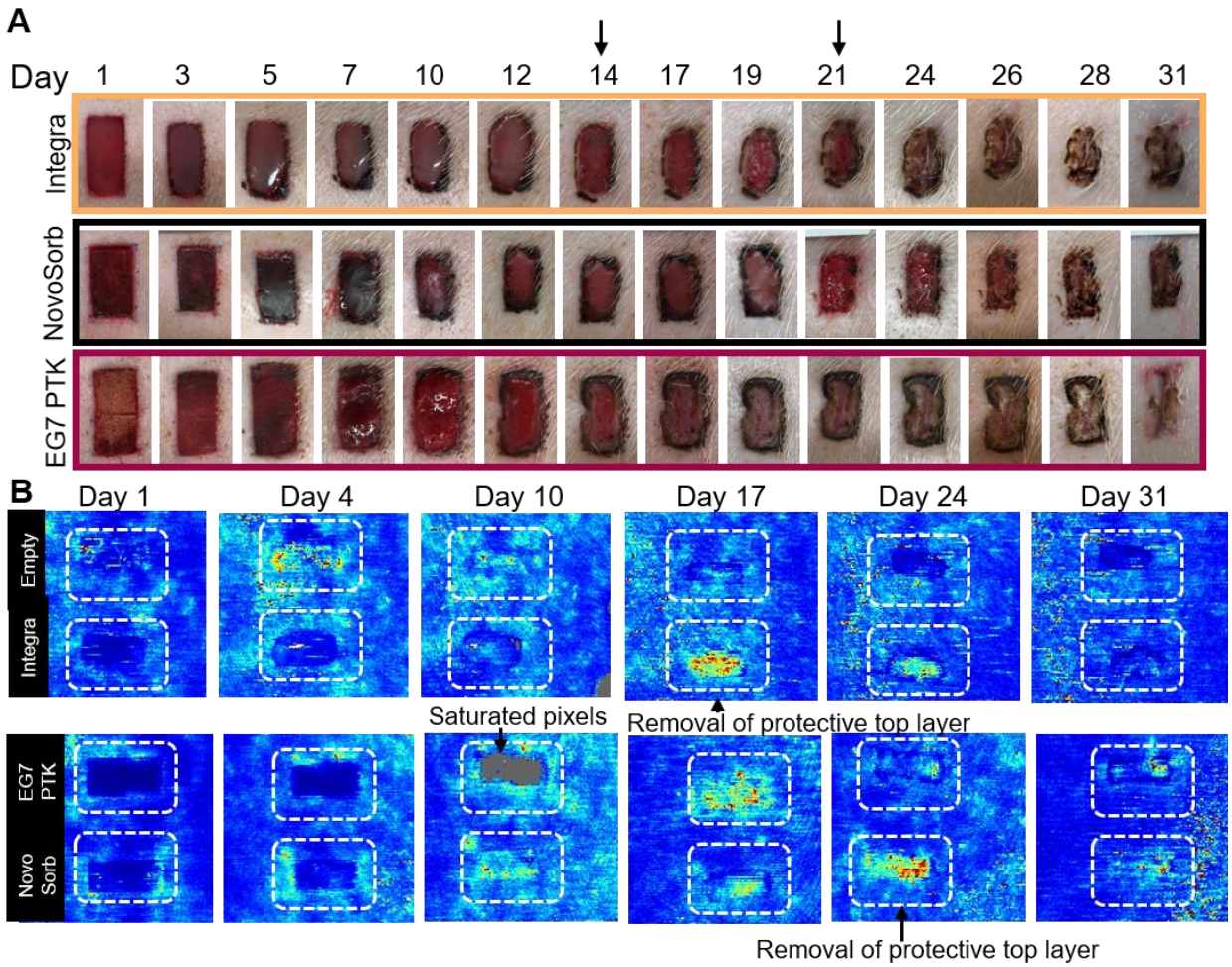

Fig. S13. Porcine skin wounds treated with EG7 PTK UR scaffold and clinically approved dermal substitutes. (A) Images of porcine skin wounds treated with Integra BWM, NovoSorb BTM or EG7 PTK-UR scaffolds showing remaining wound area and scaffold resolution. Arrows indicating removal of Integra BWM protective silicone layer on day 14 and BTM polyurethane layer on day 21. (**B**) Representative LDPI flux images showing blood perfusion within the wound. Arrows indicate removal of protective top layer of Integra and NovoSorb-treated wounds. n = 6-10 wounds.

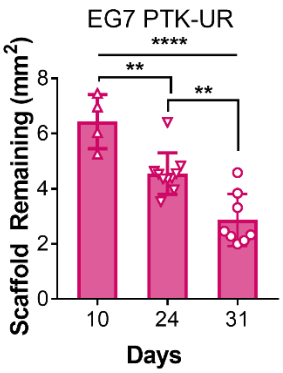

Fig. S14. In vivo degradation rate of EG7 PTK-UR scaffolds in porcine excisional skin wounds. Data presented as Mean ± SD, n = 4-10 wounds, ** $P < 0.01$, **** $P < 0.0001$ by analysis of variance (ANOVA).

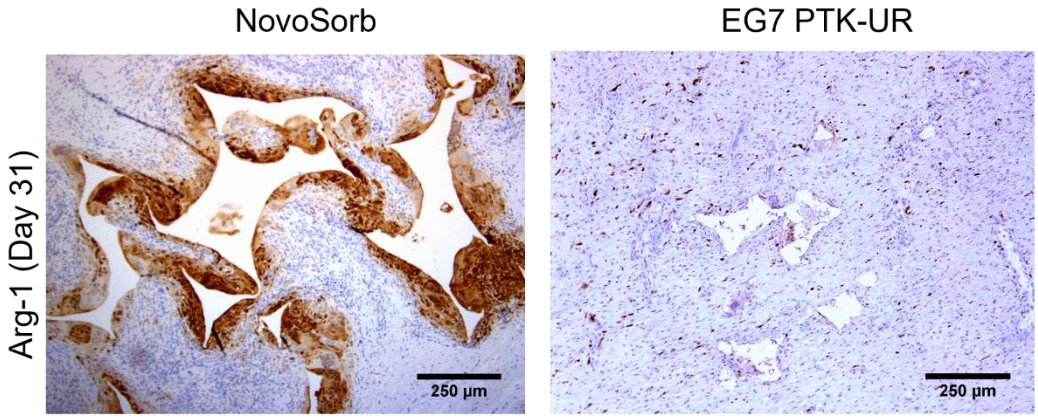

Fig. S15. Arginase-1 IHC of NovoSorb- and EG7-PTK-UR-treated wounds. Scale bar = 250 µm.

Table S1. PTK and PE-UR scaffold formulations.

	900t PE	1500t PE	EG0 PTK	EG1 PTK	EG2 PTK	EG7 PTK
Polyol	100	100	100	100	100	100
Calcium stearate	4	4	4	4	4	4
TEGOAMIN33	2.3	2.3	2.3	2.3	2.3	2.3
Water	1.5	1.5	1.5	1.5	1.5	0.5
Sulfated caster oil	1	1	1.5	1.5	1.5	2
LTI	51.8	38	27.6	27.6	27.6	23

Table S2. Wound healing scoring rubric. Rubric was used in the blinded, semi-quantitative assessment of trichome and H&E images of scaffold-treated porcine skin wounds

	Neovascularization	**Granulation Tissue Maturation**	**Epithelialization**	**Inflammation**	**Collagen**
1	Little evidence of endothelial cell ingrowth into wound site	Little evidence of mesenchymal cell infiltration; eschar predominant	Little migration of epidermis from wound edges over granulation tissue	Mostly resolved inflammatory response. No foreign body giant cells	Little or no evidence of collagen fibers. Provisional matrix consists of fibrin.
2	Angiogenic response at the wound margins and base; some extravasation	Active expansion of mesenchymal infiltration from the base and margins of the wound, accompanied by neutrophils and mononuclear cells	Initial progression of epidermal resurfacing with less than 50% coverage and hyperplasia	Residual inflammatory infiltrate with some giant cells and mild mononuclear cell infiltrate	Initial signs of collagen accumulation consisting of very fine fibrils in a random orientation.

3	> 50% of granulation tissue shows neovascularization	Continued filling of the wound site and displacement of the eschar above the wound surface	50-90% coverage of wound site. Clear polarized differentiation of epidermis	Substantial inflammatory infiltrate dominated by mononuclear cells but significant persistence of polymorphonuclear cells, frequently near wound surface	Moderate amount of collagen deposition
4	Extensive vascularization with pruning and maturation of neovessels	Accumulation of extracellular matrix, reduced density of fibroblasts, and evidence of collagen fiber organization	90-100% coverage of wound site with initiation of rete peg formation and advanced epidermal differentiation	Heavy inflammatory infiltrate resulting in impairment of healing progression, and invasion of adjacent unwounded tissue.	Loosely assembled parallel collagen fibers
5	Advanced vascular maturation with thinning of capillary networks	Extensive reconstruction of dermal architecture with absence of inflammatory infiltrate	Full keratinized epidermis with rete pegs and return of epidermal hyperplasia to thickness of adjacent, unwounded skin	Wound site dominated by inflammatory cells, including neutrophils, with consequent retardation of either granulation tissue or epidermal development.	Highly aligned collagen fiber networks with tendency to form reticular arrays. Reduced fibroblast density.